Andean Geology 53 (2): 206-224. May, 2026
doi: 10.5027/andgeoV53n2-3921

Andean Geology
www.andeangeology.cl

SPECIAL ISSUE: RESEARCH ON THE SOUTH WEST MARGIN OF GONDWANA

Miocene bimodal magmatism in the Packsaddle Volcanic Complex, Fuegian Andes, southernmost South America: evidence of oceanic-ridge subduction

*** Cristóbal Ramírez de Arellano[1]; Mauricio Calderón[2]; Benjamín Aspillaga[1]; Gonzalo Galaz[3]; Pierre Yves Descote[1]; Israel Donoso[1]; C. Mark Fanning[4]; Marly Babinski[5]; Fernando Poblete[6]**

[1] *Escuela de Ciencias de la Tierra, Universidad Andres Bello. República 220, Santiago, Chile.*
cristobal.ramirez@unab.cl; b.aspillagaortega@uandresbello.edu; pierre.descote@unab.cl; i.donosoarenas@gmail.com
[2] *Facultad de Ingeniería, Universidad del Desarrollo. Avenida Plaza 680, Las Condes, Santiago, Chile.*
mauriciocalderon@udd.cl
[3] *Departamento de Geología, Universidad de Atacama. Av. Copayapu 358, Copiapó, Chile.*
ggalaz@gmail.com
[4] *Research School of Earth Sciences, Australian National University. 142 Mills Rd, Acton ACT 0200, Canberra, Australia.*
cmarkfanning@gmail.com
[5] *Instituto de Geociências, Universidade de São Paulo. R. do Lago, 562 - Butantã, São Paulo, Brasil.*
babinski@usp.br
[6] *Departamento de Geología, Universidad de Chile. Plaza Ercilla 803, Santiago, Chile.*
ferpoble@uchile.cl

** Corresponding author: cristobal.ramirez@unab.cl*

ABSTRACT. Oceanic ridge subduction is known to generate anomalous magmatism before and during the opening of the slab window. High Sr/Y intermediate magmas and slightly alkaline basalts with transitional arc-to-intraplate (OIB-like) signatures have been reported worldwide in such tectonic settings. Southernmost South America has been affected by the subduction of several spreading ridges from the late Oligocene to the present. Here we present new geochronological, petrographic, geochemical, and isotopic data to evaluate the petrogenesis of two Lower Miocene volcanic units from the Fuegian archipelago at ~56° S, formed during subduction of the Nazca-Phoenix spreading ridge. Comparison with igneous suites related to subduction of the Chile Ridge (currently being subducted beneath central Patagonia at ~46.5° S) reveals notable similarities in timing relative to slab-window formation and in chemical signatures. We interpret the high Sr/Y chemistry as resulting from amphibole fractionation and delayed plagioclase crystallization at depth from calc-alkaline melts, with input of terrigenous material via mantle contamination or lower-crust assimilation. The slightly alkaline magmas reflect lower degrees of partial melting due to a different thermal structure of the slab-mantle wedge.

Keywords: Ridge subduction, Slab-window, Alkaline magmatism, High Sr/Y, Patagonia.

RESUMEN. Magmatismo bimodal mioceno en el Complejo Volcánico Packsaddle, Andes Fueguinos, extremo sur de América del Sur: evidencias de subducción de dorsales oceánicas. La subducción de dorsales oceánicas genera magmatismo anómalo antes y durante la apertura de la ventana astenosférica. En distintas partes del mundo, con este contexto tectónico, se han registrado magmas intermedios de alto Sr/Y y basálticos ligeramente alcalinos con rasgos transicionales entre arco e intraplaca (tipo OIB). El extremo sur de América del Sur ha sido afectado por la subducción de varias dorsales desde el Oligoceno tardío hasta el presente. Aquí exponemos nuevos datos geocronológicos, petrográficos, geoquímicos e isotópicos para evaluar la petrogénesis de dos unidades volcánicas del Mioceno Inferior del archipiélago fueguino (~56° S), formadas durante la subducción de la dorsal Nazca-Phoenix. La comparación con series ígneas relacionadas con la subducción de la dorsal de Chile (actualmente en subducción bajo la Patagonia central, ~46,5° S) revela notables similitudes en su temporalidad respecto a la formación de la ventana astenosférica y en sus firmas químicas. Interpretamos la química de alto Sr/Y como el resultado de fraccionamiento de anfíbola y de la cristalización tardía de plagioclasa en profundidad, a partir de magmas calcoalcalinos, con aporte de material terrígeno vía contaminación del manto o asimilación de la corteza inferior. Los magmas ligeramente alcalinos reflejan menores grados de fusión parcial debido a una estructura térmica de la cuña mantélica distinta.

Palabras clave: Subducción de dorsales, Ventana astenosférica, Magmatismo alcalino, Alto Sr/Y, Patagonia.

1. Introduction

The chemistry of igneous rocks from subduction settings typically follows a calc-alkaline differentiation trend originating from basaltic primary melts (Wilson, 1989). Nevertheless, a variety of subduction-related primary magmas belonging to different magma series have been described (Schmidt and Jagoutz, 2017). In tectonic settings where oceanic spreading ridges are subducted, two distinct series often coexist: slightly alkaline transitional magmas derived from low-silica basaltic primary melts, and magmas produced by andesitic primary melts, often with high Sr/Y ratios and following a subalkaline trend (Yogodzinski *et al.*, 2001; Gómez-Tuena *et al.*, 2018; Ramírez de Arellano *et al.*, 2021; Zhen *et al.*, 2025).

Southern South America has been influenced by the subduction of several spreading ridges from the late Oligocene to the present. Miocene volcanic and plutonic rocks with transitional (slightly alkaline) composition have been reported between 47° and 50° S (Ramos and Kay, 1992; Gorring *et al.*, 1997; D'Orazio *et al.*, 2004; Guivel *et al.*, 2006; Corbella and Lara, 2008). These rocks are roughly coeval with high Sr/Y andesites (Kay *et al.*, 1993; Ramos *et al.*, 2004; Orihashi *et al.*, 2013). With ages from 12 Ma to present, they predate the opening of the slab window associated with the subduction of the Chile Ridge (Kay *et al.*, 1993; Ramírez de Arellano *et al.*, 2012, 2021). Similarly, in southernmost South America, at the latitude of Tierra del Fuego (55° S), Miocene basaltic and andesitic rocks showing both compositional types have been reported on the continental margin of the Scotia Plate. They have been grouped as the Packsaddle Volcanic Complex (PVC) exposed on different islands of the Fuegian archipelago (Suárez *et al.*, 1985; Fig. 1). Available geochemical data are however limited, and ages are poorly constrained to *ca.* 18-21 Ma (K-Ar dating; Puig *et al.*, 1984). Regional palaeogeographic reconstruction indicates that the Nazca-Phoenix spreading ridge has been located off Tierra del Fuego since *ca.* 30 Ma (Eagles and Jokat, 2014), implying a spatial and temporal relation between the Nazca-Phoenix Ridge and the PVC.

Given these Patagonian occurrences linked to the subduction of two different spreading-ridges, it remains unclear whether the two magma types formed simultaneously or reflect a magmatic transition. It is also unclear which common conditions favor their genesis. Here, we provide new data on field relations of volcanic and volcaniclastic units, petrography, geochemistry and geochronology of the PVC to evaluate its petrogenesis and the causal relationship of transitional (slightly alkaline) and the high Sr/Y andesitic magmatism to spreading-ridge subduction.

2. Tectonic and geologic setting

The subduction of several oceanic spreading ridges occurred along the southernmost segment of South America from the Palaeogene to the Neogene (Fig. 2). The Farallon-Phoenix Ridge migrated southward relative to South America from the Mesozoic and reached the Tierra del Fuego region (~53° S) by the Oligocene Epoch, at *ca.* 30 Ma (Pardo-Casas and Molnar, 1987; Eagles and Jokat, 2014; Eagles and Scott, 2014). Following the breakup of the Farallon Plate and a major plate reorganization in the late Oligocene (*ca.* 26 Ma), the Farallon-Phoenix Ridge became known as the Nazca-Phoenix Ridge (NAZ-PHO) and continued to be subducted beneath Tierra del Fuego until *ca.* 20 Ma (*e.g.,* Eagles and Jokat, 2014; Eagles and Scott, 2014). Migration concluded with the subduction of the triple junction between the Nazca, Phoenix, and Antarctic plates, after which two separate ridges were subducted (Eagles and Jokat, 2014; Eagles and Scott, 2014; see figure 2). The Nazca-Antarctica Ridge migrated rapidly northward to its present position near the Taitao Peninsula (~46.5° S) and is now referred to as the Chile Ridge (Cande and Leslie, 1986; Pardo-Casas and Molnar, 1987; Breitsprecher and Thorkelson, 2009). It is proposed that the Antarctic-Phoenix Ridge (ANT-PHO) migrated southward, from ~54° to 57.5° S along the southwestern margin of the Scotia Plate (Eagles and Jokat, 2014; Eagles and Scott, 2014; see figure 2). The separate subduction of the Chile Ridge and the ANT-PHO Ridge produced distinct structural and magmatic effects in their respective segments of the margin. Ramírez de Arellano *et al.* (2021) proposed the terms Patagonian and Fuegian domains, separated by the South America-Scotia plate boundary at ~53° S, to describe the contrasting chemical signatures in these two Andean segments.

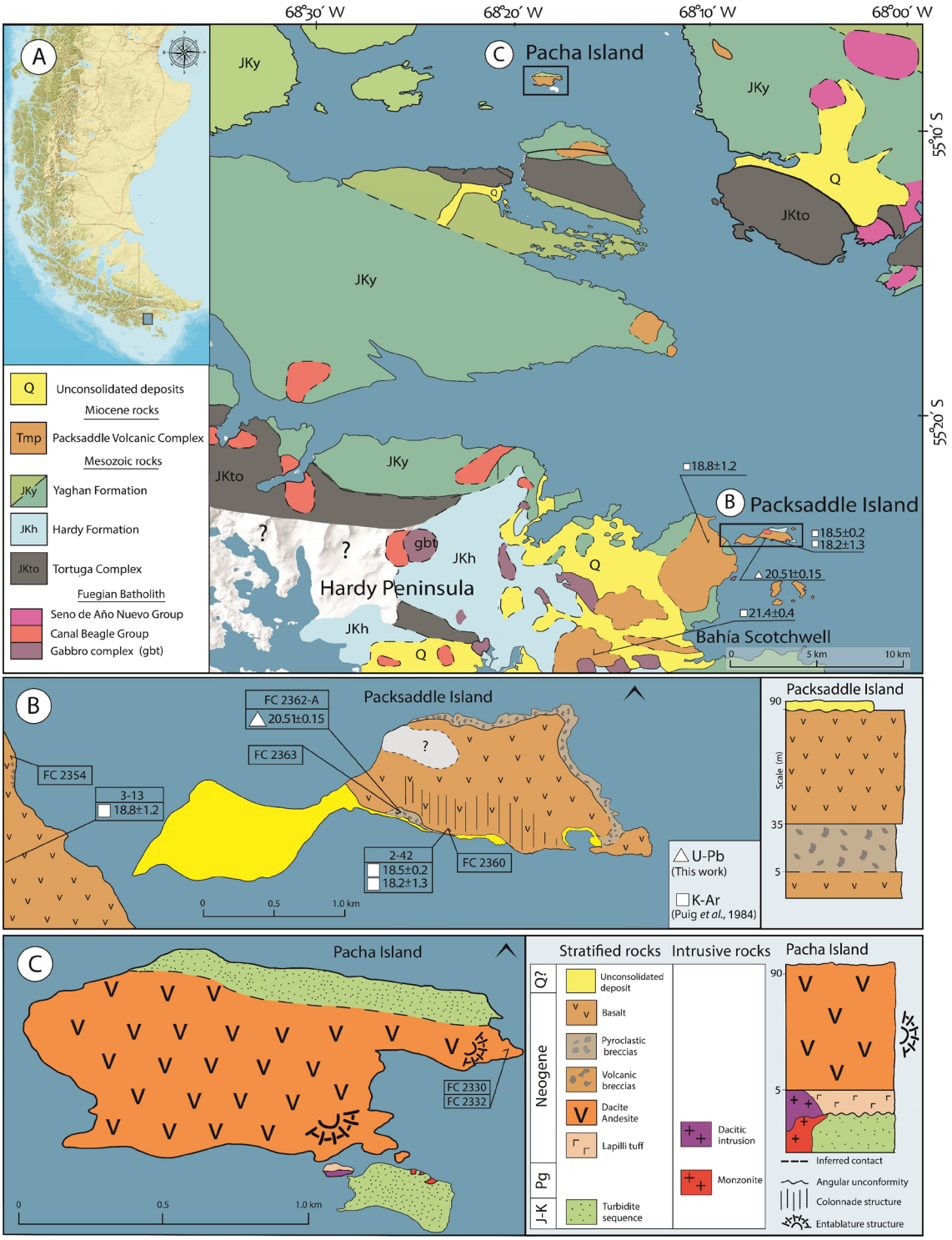

FIG. 1. Geological map of Packsaddle and Pacha islands and surrounding areas. **A** is after Suárez *et al.* (1985) with regional units and locations of samples dated by Puig *et al.* (1984). **B** and **C** are lithological maps produced in this work, with location of samples used for geochemistry and U-Pb SHRIMP zircon dating; schematic stratigraphic columns are shown to the right. All ages in Ma.

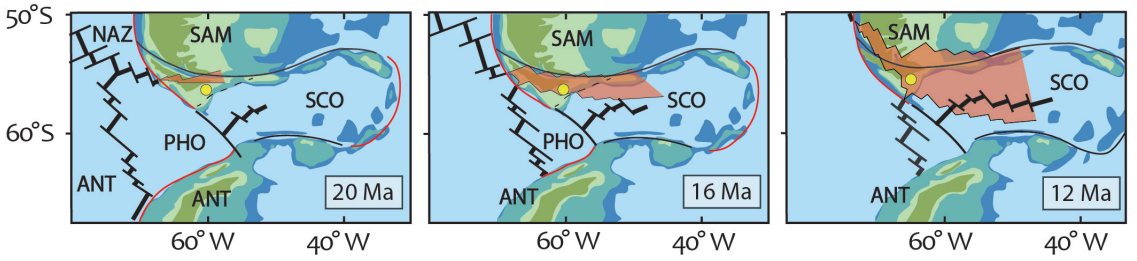

FIG. 2. Plate-tectonic evolution of the Fuegian region in southernmost South America after Eagle and Jokat (2014), showing subduction of the Nazca (NAZ), Phoenix (PHO), and Antarctic (ANT) plates beneath the South America (SAM) and Scotia (SCO) plates at 20, 16, and 12 Ma. The slab window (brownish red domain) follows Breitsprecher and Thorkelson (2009). The yellow circle marks the study area: at 20 Ma it laid above the Phoenix Plate slab, whereas by 16 and 12 Ma it laid above the slab window.

In the Patagonian domain (north of 53° S), Chile Ridge subduction at *ca.* 16 Ma is invoked to explain rapid exhumation and development of the Magallanes Fold-and-Thrust Belt (Ramos, 2005; Stevens-Goddard and Fosdick, 2019; Muller *et al.*, 2024). In this segment, the exhumation exposes Lower Miocene calc-alkaline plutonic rocks (Hervé *et al.*, 2007), where they crop out in ranges reaching up to ~3,000 m a.s.l. (Nullo *et al.*, 1978; Ramos, 2005; Ramírez de Arellano *et al.*, 2012). Plutonic rocks from the batholith and satellite plutons record progressive eastward arc migration during the Early Miocene (Espinoza *et al.*, 2010; Ramírez de Arellano *et al.*, 2012). During the Late Miocene, after 12 Ma, the eastern Andes of Patagonia experienced 'transitional' magmatism, becoming increasingly enriched in alkalis compared to the typical calc-alkaline products of the batholith (*e.g.,* Gorring *et al.*, 1997; D'Orazio *et al.*, 2004; Guivel *et al.*, 2006; Corbella and Lara, 2008). Coeval (14 to 11 Ma) volcanic and subvolcanic andesites with high Sr/Y ratios (>20) have been reported along this arc domain as well (Kay *et al.*, 1993; Ramos *et al.*, 2004).

In the Fuegian domain (that is, south of 53° S), Lower Miocene sedimentary and volcanic rocks are still preserved, implying lower exhumation rates with respect to the Patagonian domain. Suárez *et al.* (1985) described two Miocene (Burdigalian) volcanic units enclosed within the Packsaddle Volcanic Complex (PVC). The sparse chemistry of these rocks suggests that these two units could resemble the alkaline-transitional and the high Sr/Y rocks from the Patagonian domain (Puig *et al.*, 1984; Ramírez de Arellano *et al.*, 2021).

The PVC was studied by Hervé *et al.* (1984), Puig *et al.* (1984), and Suárez *et al.* (1985), in the context of a regional (1:250,000 scale) geological study (Fig. 1A). The PVC unconformably overlies deformed Upper Jurassic to Lower Cretaceous igneous rocks and deformed sedimentary rocks related to the Rocas Verdes marginal basin (Dalziel *et al.*, 1974; Suárez *et al.*, 1985; Stern and de Witt, 2003; Calderón *et al.*, 2007). At some places, the PVC also overlies Palaeogene plutonic rocks from the Seno de Año Nuevo Group of Suárez *et al.* (1985), who described two units of andesites and alkaline basalts. A PVC andesite was dated at 21.4±0.2 Ma by K-Ar in whole-rock (average of 21.4±0.2 and 21.4±0.4 Ma; Puig *et al.*, 1984; see figure 1A). These rocks crop out on Hardy Peninsula (Fig. 1A) as isolated bodies and were described as porphyritic andesites and volcanic breccias (Suárez *et al.*, 1985). Alkaline basalts cropping out on Packsaddle Island were dated by K-Ar in whole-rock at 18.5±0.2 Ma (average of 18.2±1.3, 18.5±0.2, and 18.8±1.2 Ma; Puig *et al.*, 1984; see figure 1A), indicating that they probably postdate the andesitic rocks, although the contact relationship between these two volcanic units was not reported.

In more recent fieldwork conducted by the authors, volcanic and volcaniclastic rocks of the PVC were studied at three localities: Packsaddle Island, Pacha Island, and Hardy Peninsula on Hoste Island (Fig. 1A). In a broad sense, the representative lithologies are olivine-bearing basalts on Packsaddle Island and hornblende-bearing dacites on Pacha Island (Fig. 1B, C).

The outcrops at Packsaddle Island are mainly composed of a 30 m-thick basalt layer, well exposed along the southern side of the island, with a characteristic colonnade structure (Fig. 3A). Previous studies interpreted this body as a lava flow, yet without providing a detailed description of its contacts with adjacent rocks. In our study, newly identified field relationships suggest that it may

instead correspond to a hypabyssal intrusion, likely a sill, emplaced within a succession of volcanic and volcaniclastic rocks. The lower contact of the basaltic unit is sharp and markedly irregular, truncating the underlying volcanic breccia with a sharp cross-cutting relationship (Fig. 3B). The breccia layers have a minimum thickness of 20 m (Fig. 3C). They are characterized by a pyroclastic matrix that comprises up to 70 vol.% of the rock (60-80% lapilli and 20-40% ash) and contain andesitic-dacitic clasts and subordinate crystalline tuff fragments ranging from a few cm to blocks over two m in diameter. Abundant clasts of hornblende-bearing dacite, like those from Pacha Island, are found in these breccias. The volcanic rocks from Packsaddle Island are overlain by an unconsolidated (Holocene?), fine-grained and matrix-supported marine-lacustrine deposit (Fig. 1B). This deposit contains subrounded polymictic clasts (<5 mm size) and marine fossils, such as bivalves.

On Hardy Peninsula (Fig. 1A, B), lava flows, breccias and subvolcanic dikes alternate with gabbros and diorites of satellite intrusions of the Fuegian Batholith. Volcanic rocks from the PVC could easily be confused with the Jurassic rocks from the Hardy Formation, which consist of intermediate to felsic lavas and breccias.

The Pacha Island (Fig. 1C), located ~30 km north of Packsaddle Island, is mainly composed of hornblende-bearing dacitic lavas, with a characteristic entablature structure, overlying deformed rocks of the Yaghan Formation and isolated monzonitic plutons of the Fuegian Batholith. Small outcrops (<10 m^2) of tuff can be observed at the base of the lavas.

Following Suárez *et al.* (1985) and the recommendations of Ricci *et al.* (1993), we propose the name 'Packsaddle Basalts' for the olivine basalts and volcaniclastic breccias of Packsaddle Island and the isolated outcrops on Hardy Peninsula, and 'Pacha Dacites' for the hornblende-bearing andesites and dacites of Pacha Island and Hardy Peninsula. Both units are part of the PVC. Schematic stratigraphic columns with sample locations are shown in figure 1.

3. Methods

Forty samples from the PVC, including samples from the Packsaddle and Pacha islands and the surrounding areas, were petrographically analysed under a Nikon Eclipse E200 polarizing microscope to identify the texture and modal mineralogy of volcanic (lavas, tuff and breccias) and subvolcanic rocks.

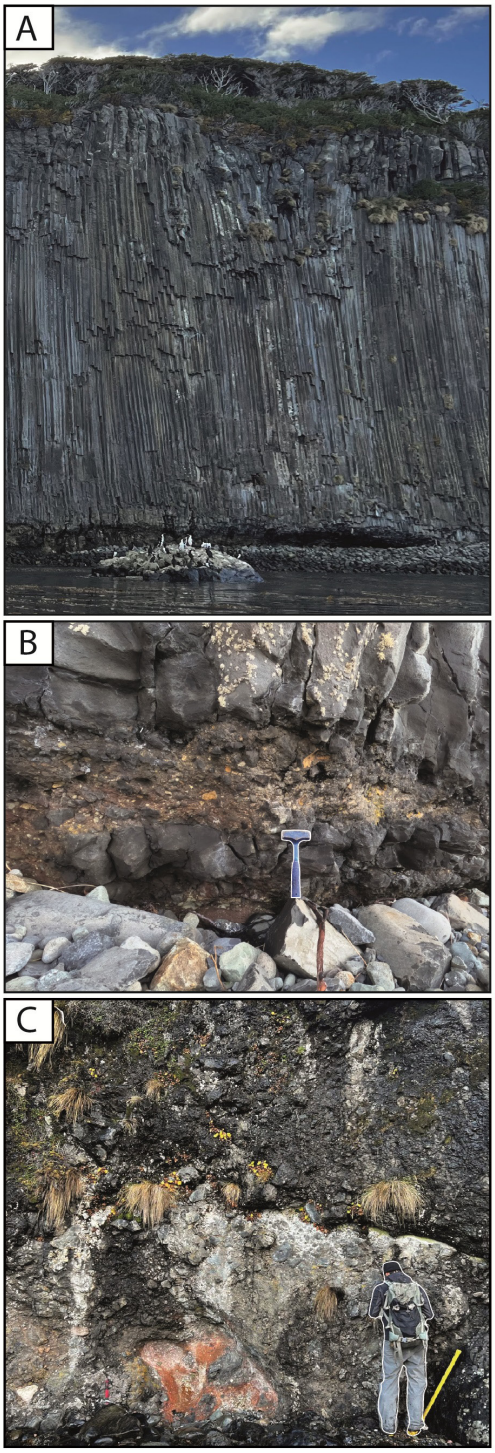

FIG. 3. Field observations on Packsaddle Island. **A.** Columnar jointing in the main basalt sill. **B.** Detail of the contact between the lower breccia and the overlying basalt, showing the basalt crosscutting the breccia. **C.** Lower pyroclastic breccia, which locally reaches up to 30 m thickness; note the block sizes and distribution.

New whole-rock geochemical data from nine samples of the PVC are presented in Table 1. They include two clasts of hornblende-biotite dacite of the lower breccia from Packsaddle Island, an olivine basalt from the same island, two dacites from Pacha Island, and four samples from Hardy Peninsula (two plutonic, a micro-gabbro and an olivine basalt). These samples were analysed for major and trace element compositions using ICP-AES (inductively coupled plasma atomic emission spectroscopy) and ICP-MS (inductively coupled plasma mass spectroscopy) at Activation Laboratories Ltd. (Actlabs) in Vancouver, Canada. Different element ratios were used to classify the volcanic units and evaluate petrogenetic processes (see below).

A new U-Pb zircon age was obtained for a clast of hornblende-biotite dacite of the Pacha Dacite unit, from the volcanic breccia at Packsaddle Island (sample FC2362-A), using SHRIMP II (sensitive high-resolution ion microprobe) at the Research School of Earth Sciences, Australian National University, in Canberra, Australia. Analytical techniques essentially follow those given in Williams (1998), comprising six scans through the mass spectrum, with the Temora 1 reference zircon (Black *et al.*, 2003) used to calibrate the U/Pb ratios. The data were processed using the SQUID add-in Excel Macro of Ludwig (2000) and corrections for common Pb made using the measured $^{238}U/^{206}Pb$ and $^{207}Pb/^{206}Pb$ ratios following Tera and Wasserburg (1972) as outlined in Williams (1998). Results are shown in Table 2. Uncertainties in weighted mean age calculations are reported at the 2σ level. The geological time scale used follows the Chronostratigraphic Chart 2022 by IUGS-ICS.

Sr and Nd isotope determinations of a dacite breccia clast and an olivine basalt from Packsaddle Island, one micro-gabbro from Hardy Peninsula, and one dacite from Pacha Island were carried out at the Geochronological Research Centre at Universidade de São Paulo, Brazil (Table 3). Rock powders (100 mg) were dissolved in Savillex beakers with HF and HNO_3 on a hot plate for 5 days at 110 °C, dried down on a hot plate, and the residue was dissolved in 6 M HCl at 110 °C for 24 hours. The HCl solution was dried down and converted to nitrates with concentrated HNO_3. Sr was separated using Eichrom Sr-Spec® resin and eluted with 0.05 M HNO_3. Nd was purified using two steps of ion-exchange columns with RE-Spec® and LN-Spec® resins; Nd was eluted in 0.26 M HCl. The Sr isotope ratios were determined on a Triton TIMS (thermo-ionization mass spectrometer) in dynamic mode. The ratios were normalized to $^{86}Sr/^{88}Sr=0.1194$, and the NBS987 standard analysed during this study gave a mean $^{87}Sr/^{86}Sr$ value of 0.710250±0.000018 (2σ). The Sr blanks were about 128 pg. The Nd isotope ratios were determined on a Thermo Scientific Neptune multicollector ICP-MS. The ratios were normalized to $^{146}Nd/^{144}Nd=0.7219$, and the $^{143}Nd/^{144}Nd$ average for the JNdi-1 standard analysed during this study was 0.512197±0.000004 (2σ). The analytical blanks were about 270 pg.

4. Results

4.1. Petrography of the PVC

The olivine basalts from Packsaddle Island constitute the uppermost, larger, unit of the island. They exhibit a pilotaxitic texture, with olivine and plagioclase phenocrysts (Fig. 4A). The groundmass occupies ~90% of the rock volume and consists primarily of plagioclase (65%), minor pyroxene and olivine microliths (5%), and glass (30%).

The lower stratigraphic unit observed at Packsaddle is of pyroxene basalts located in the east of the island. These basalts comprise cumulates of clinopyroxenes and minor olivine in a microcrystalline groundmass mainly composed of plagioclase microliths, clinopyroxene, and glass. Breccias overlying the lower basalts show variation in the size and nature of their clasts, but all have a vitreous-crystalline matrix with abundant clasts of porphyritic hornblende-bearing andesites and dacites (Fig. 4B). The dated crystalline tuff (FC2362-A) presents abundant crystals (~30%, <1mm), mainly plagioclase, hornblende, and minor biotite in a vitreous-crystalline matrix.

The two dacite samples (66 wt.% SiO_2) from Pacha Island exhibit a porphyritic texture, with 75-85% groundmass, predominantly pilotaxitic, consisting of plagioclase microliths, along with granular quartz, and minor volcanic glass and oxides (Fig. 4C). Phenocrysts are primarily hornblende and plagioclase (3:1). Hornblende is subhedral (0.3-1.5 mm), in some cases poikilitic, enclosing plagioclase crystals. Conversely, euhedral to subhedral plagioclase phenocrysts (0.3 to 1.0 mm) show Carlsbad twinning and subtle compositional zoning. Sieve textures and reabsorbed rims are common.

TABLE 1. WHOLE-ROCK GEOCHEMISTRY OF THE PACKSADDLE VOLCANIC COMPLEX.

Locality	Packsaddle Island							Pacha Island		Hardy Peninsula									
Sample N°	**FC2362-A**	**FC2363**	**FC2360**	**11TU-5801**	**11TU-5808**	**2-42**	**686**	**FC2330**	**FC2332**	**FC2349**	**FC2351**	**FC2352**	**FC2354**	**3-13**	**3-12-c**	**3-14**	**3-15**	**182**	**523-1**	**1-51**
Rock type	**Dacite clast**	**Dacite clast**	**Ol-basalt**	**Basalt**	**Basalt**	**Basalt**	**Basalt**	**Dacite**	**Dacite**	**Micro-gabbro**	**Diorite**	**Gabbro**	**Ol-basalt**	**Basalt**	**Andesite**	**Andesite**	**Dacite**	**Dacite**	**Dacite**	**Dacite**
Latitude	**55,402**	**55,402**	**55,403**	**55,4**	**55,4**			**55,13**	**55,128**	**55,427**	**55,421**	**55,421**	**55,396**							
Longitude	**68,080**	**68,080**	**68,138**	**68,1**	**68,1**			**68,289**	**68,287**	**68,114**	**68,111**	**68,111**	**68,138**							
Reference*	**This work**	**This work**	**This work**	**R.2021**	**R.2021**	**P.1984**	**P.1984**	**This work**	**This work**	**This work**	**This work**	**This work**	**This work**	**P.1984**	**P.1984**	**P.1984**	**P.1984**	**P.1984**	**P.1984**	**P.1984**
SiO_2 [wt.%]	66.18	64.81	50.21	49.89	49.22	49.67	50.21	66.02	66.07	51.55	57.80	45.11	50.02	49.10	62.94	62.58	63.53	67.02	64.18	57.27
TiO_2 [wt.%]	0.57	0.66	1.72	1.80	1.81	1.89	1.83	0.57	0.58	0.70	0.61	1.40	1.54	1.68	0.74	0.72	0.73	0.60	0.83	0.79
Al_2O_3 [wt.%]	17.47	17.74	15.56	16.04	16.30	15.97	16.03	16.69	16.46	17.05	18.32	16.77	16.41	17.06	18.77	18.87	18.92	16.93	17.75	18.15
FeO* [wt.%]	3.45	4.13	8.27	8.27	8.63	8.22	7.93	3.97	3.81	8.22	7.13	12.27	8.34	9.04	4.51	4.49	4.27	3.48	4.72	6.29
MnO [wt.%]	0.08	0.08	0.20	0.17	0.19	0.23	0.16	0.05	0.08	0.33	0.22	0.27	0.15	0.18	0.12	0.10	0.10	0.08	0.15	0.13
MgO [wt.%]	1.17	1.39	9.02	8.78	8.93	9.21	8.83	2.07	2.00	8.62	3.31	8.70	9.62	7.94	1.97	1.97	1.38	1.19	1.24	4.71
CaO [wt.%]	3.99	4.39	9.11	9.28	9.25	9.22	9.13	5.00	5.45	10.36	7.78	12.82	9.29	10.58	5.67	5.72	5.54	5.28	5.57	7.84
Na_2O [wt.%]	4.17	4.68	3.85	3.73	3.60	3.63	3.85	3.82	3.79	2.60	3.25	2.13	3.13	3.31	3.94	4.20	4.28	3.78	3.92	3.65
K_2O [wt.%]	2.72	1.94	1.47	1.53	1.51	1.41	1.52	1.63	1.59	0.35	1.40	0.26	1.01	0.77	1.14	1.13	1.14	1.49	1.55	0.94
P_2O_5 [wt.%]	0.21	0.19	0.51	0.52	0.57	0.49	0.51	0.17	0.16	0.15	0.17	0.20	0.41	0.30	0.20	0.20	0.10	0.15	0.10	0.20
LOI [wt.%]	2.44	1.07	1.1	1.5	1.62	1.86	0	3.29	2.74	2.91	3.71	1.28	2.67	1.84	1.78	1.91	2.36	0	0	0.93
Original Total	**97.51**	**98.79**	**97.64**	**100.30**	**100.40**	**96.50**	**98.58**	**96.10**	**97.67**	**98.98**	**94.56**	**98.37**	**97.43**	**96.15**	**97.00**	**96.96**	**96.24**	**100.42**	**96.92**	**97.76**
Sc [ppm]	5	7	24	25	24	-	-	8	8	31	15	50	26	-	-	-	-	-	-	-
V [ppm]	92	52	227	216	221	196	-	75	76	230	160	491	210	197	83	86	84	-	-	126
Cr [ppm]	< 20	20	340	310	300	300	-	30	60	420	80	260	380	258	5	5	5	-	-	181
Co [ppm]	9	9	37	38	37	-	-	9	9	30	15	46	36	-	-	-	-	-	-	-
Ni [ppm]	< 20	< 20	220	170	160	115	-	30	50	140	40	130	210	78	3	3	3	-	-	91
Cu [ppm]	20	30	80	-		-	-	30	30	120	40	10	70	-	-	-	-	-	-	-
Zn [ppm]	50	40	60	70	70	-	-	50	60	200	80	120	70	-	-	-	-	-	-	-
Ga [ppm]	17	17	16	-	-	-	-	16	17	16	16	17	16	-	-	-	-	-	-	-
Ge [ppm]	1.2	1.3	1.2	-	-	-	-	0.9	1.1	1.4	0.9	1.6	1	-	-	-	-	-	-	-
Rb [ppm]	82	49	21	18	18	16	-	51	55	6	26	3	11	11	35	35	37	-	-	23
Sr [ppm]	570	607	923	873	946	914	-	598	656	393	493	314	823	961	714	695	721	-	-	901
Y [ppm]	11	13	20	21	22	24	-	9	9	15	17	26	19	25	15	14	13	-	-	15
Zr [ppm]	133	131	166	161	175	174	-	92	94	46	71	38	167	141	103	102	101	-	-	87
Nb [ppm]	10	9	19	21	19	24	-	10	11	2	3	1	11	9	5	5	4	-	-	7
Cs [ppm]	4.0	0.5	0.6	0.8	0.7	-	-	1.1	2.5	0.6	1.8	0.6	0.3	-	-	-	-	-	-	
Ba [ppm]	745	730	566	513	574	469	-	496	500	181	648	71	293	425	490	497	509	-	-	485
La [ppm]	20.8	21.1	28.4	29.2	29.8	30.0	-	14.5	14.9	5.5	7.1	4.0	21.8	23.0	5.0	7.0	6.0	-	-	25.0
Ce [ppm]	38.7	36.8	55.9	58.7	59.5	-	-	26.3	27.9	12.9	16.3	12.7	45.6	-	-	-	-	-	-	-
Pr [ppm]	4.02	3.84	6.15	6.68	6.83	-	-	2.72	2.87	1.70	2.05	1.92	4.99	-	-	-	-	-	-	-
Nd [ppm]	15.3	15.8	26.7	26.1	25.9	-	-	10.7	11.6	8.9	10.1	11.6	21.6	-	-	-	-	-	-	-
Sm [ppm]	2.55	2.62	4.81	4.78	4.97	-	-	1.86	2.02	2.13	2.58	3.43	4.10	-	-	-	-	-	-	-
Eu [ppm]	0.76	0.88	1.43	1.67	1.80	-	-	0.56	0.65	0.77	0.80	1.12	1.32	-	-	-	-	-	-	-
Gd [ppm]	2.14	2.42	4.17	3.88	4.15	-	-	1.78	1.90	2.24	2.69	4.20	3.76	-	-	-	-	-	-	-
Tb [ppm]	0.34	0.40	0.66	0.67	0.67	-	-	0.29	0.30	0.42	0.47	0.76	0.63	-	-	-	-	-	-	-
Dy [ppm]	1.97	2.19	3.82	4.02	4.07	-	-	1.72	1.79	2.78	2.94	4.82	3.64	-	-	-	-	-	-	-
Ho [ppm]	0.39	0.42	0.71	0.75	0.76	-	-	0.33	0.35	0.56	0.60	1.01	0.69	-	-	-	-	-	-	-
Er [ppm]	1.16	1.24	2.01	2.09	2.17	-	-	0.98	0.95	1.72	1.95	2.99	2.03	-	-	-	-	-	-	-
Tm [ppm]	0.180	0.196	0.297	0.290	0.300	-	-	0.135	0.145	0.261	0.310	0.423	0.293	-	-	-	-	-	-	-
Yb [ppm]	1.22	1.32	1.91	1.87	2.05	-	-	0.86	1.00	1.72	2.16	2.76	1.94	-	-	-	-	-	-	-
Lu [ppm]	0.189	0.208	0.301	0.28	0.3	-	-	0.132	0.161	0.251	0.327	0.436	0.315	-	-	-	-	-	-	-
Hf [ppm]	3.2	3.2	3.5	3.6	3.6	-	-	2.1	2.5	1.3	1.8	1.3	3.5	-	-	-	-	-	-	-
Ta [ppm]	0.89	0.88	1.26	1.32	1.38	-	-	0.89	0.93	0.13	0.20	0.06	0.81	-	-	-	-	-	-	-
Tl [ppm]	0.52	0.14	0.11	-	-	-	-	0.25	0.28	0.05	0.21	0.11	0.06	-	-	-	-	-	-	-
Pb [ppm]	18	19	7	18	7	-	-	12	13	10	8	< 5	6	-	-	-	-	-	-	-
Th [ppm]	8.34	7.66	4.44	4.31	4.06	-	-	5.44	5.83	1.35	1.83	0.26	3.09	-	-	-	-	-	-	-
U [ppm]	2.81	2.3	1.1	1.11	1.09	-	-	2.1	2.38	0.48	0.62	0.11	0.81	-	-	-	-	-	-	-
Mg#/100	0.38	0.37	0.66	0.65	0.65	0.67	0.66	0.48	0.48	0.65	0.45	0.56	0.67	0.61	0.44	0.44	0.37	0.38	0.32	0.57
K/Na	0.73	0.47	0.43	0.27	0.28	0.43	0.44	0.48	0.47	0.15	0.48	0.14	0.36	0.26	0.33	0.30	0.30	0.44	0.44	0.29
Sr/Y	50.4	47.1	46.6	42.4	42.2	38.1	-	65.7	69.8	26.4	29.0	12.3	43.5	38.4	47.6	49.6	55.5	-	-	60.1
Rb/Ba	0.11	0.07	0.04	0.04	0.03	0.03	-	0.10	0.11	0.03	0.04	0.04	0.04	0.03	0.07	0.07	0.07	-	-	0.05
Ba/Nb	76.8	81.1	29.9	24.0	29.6	19.5	-	50.6	44.2	113.1	249.2	71.0	26.4	47.2	98.0	99.4	127.3	-	-	69.3
Ce/Pb	2.2	1.9	8.0	3.3	8.5	-	-	2.2	2.1	1.3	2.0	-	7.6	-	-	-	-	-	-	-
La/Th	2.49	2.75	6.40	6.77	7.34	-	-	2.67	2.56	4.05	3.87	15.46	7.06	-	-	-	-	-	-	-

*It includes previously published data from P.1984 (Puig *et al.*, 1984) and R.2021 (Ramírez de Arellano *et al.*, 2021); The table also includes the element's ratios mentioned in the text.

TABLE 2. SUMMARY OF U-Pb SHRIMP ZIRCON DATING FROM SAMPLE FC2362-A.

							Total				Radiogenic		Age [Ma]	
Grain spot	U [ppm]	Th [ppm]	Th/U	$^{206}Pb^*$ [ppm]	$^{204}Pb/^{206}Pb$	f_{206} [%]	$^{238}U/^{206}Pb$	±	$^{207}Pb/^{206}Pb$	±	$^{206}Pb/^{238}U$	±	$^{206}Pb/^{238}U$	±
1.1	180	68	0.38	0.5	-	<0.01	309.88	9.82	0.0450	0.0091	0.00323	0.00011	20.81	0.70
2.1	3,025	2,977	0.98	8.2	-	0.34	317.88	3.99	0.0491	0.0016	0.00314	0.00004	20.18	0.26
3.1	2,051	998	0.49	5.6	-	0.13	314.84	4.27	0.0475	0.0019	0.00317	0.00004	20.42	0.28
4.1	358	128	0.36	1.0	-	0.27	312.65	7.40	0.0485	0.0067	0.00319	0.00008	20.53	0.52
5.1	182	54	0.30	2.5	-	0.50	61.43	1.10	0.0520	0.0029	0.01620	0.00030	103.59	1.88
6.1	1,326	635	0.48	3.6	0.001794	0.11	317.41	4.81	0.0473	0.0024	0.00315	0.00005	20.25	0.31
7.1	2,070	591	0.29	5.6	0.000563	0.45	317.06	4.30	0.0500	0.0019	0.00314	0.00004	20.21	0.28
8.1	1,313	596	0.45	3.6	-	0.11	310.12	4.71	0.0473	0.0023	0.00322	0.00005	20.73	0.32
9.1	738	302	0.41	2.0	0.002040	0.54	317.34	7.76	0.0507	0.0031	0.00313	0.00008	20.17	0.50
10.1	2,740	4.161	1.52	7.6	0.000312	0.47	309.26	3.98	0.0502	0.0017	0.00322	0.00004	20.71	0.27
11.1	3,106	956	0.31	8.7	0.000321	0.44	308.21	5.78	0.0499	0.0016	0.00323	0.00006	20.79	0.39
12.1	2,765	886	0.32	7.7	-	0.13	307.47	4.05	0.0475	0.0016	0.00325	0.00004	20.90	0.28
13.1	1,297	731	0.56	3.7	0.001382	2.04	304.18	4.62	0.0626	0.0027	0.00322	0.00005	20.73	0.32
14.1	224	109	0.48	0.6	0.002989	0.59	308.13	9.79	0.0511	0.0111	0.00323	0.00011	20.77	0.72
15.1	2,336	561	0.24	6.5	0.000244	0.43	308.28	4.05	0.0498	0.0019	0.00323	0.00004	20.79	0.28
16.1	1,378	618	0.45	3.8	0.000913	0.32	311.96	4.73	0.0489	0.0024	0.00320	0.00005	20.57	0.32
17.1	1,354	631	0.47	3.8	0.000619	<0.01	305.13	4.84	0.0453	0.0023	0.00328	0.00005	21.12	0.34
18.1	2,186	1.100	0.50	6.0	-	0.07	311.23	7.03	0.0470	0.0018	0.00321	0.00007	20.67	0.47
19.1	562	360	0.64	1.5	0.001989	0.36	317.02	6.78	0.0492	0.0036	0.00314	0.00007	20.23	0.44
20.1	631	240	0.38	1.7	0.001285	1.05	313.83	6.04	0.0547	0.0036	0.00315	0.00006	20.29	0.40
21.1	750	234	0.31	2.0	-	0.34	323.78	6.22	0.0491	0.0032	0.00308	0.00006	19.81	0.39
22.1	334	431	1.29	0.9	-	2.61	325.15	8.71	0.0671	0.0056	0.00300	0.00008	19.28	0.53

Notes:

1. Uncertainties given at the one σ level.
2. Error in Temora 1 reference zircon calibration was 0.45% for the analytical session (not included in above errors but required when comparing data from different mounts)
3. f_{206} [%] denotes the percentage of ^{206}Pb that is common Pb.
4. Correction for common Pb for the U/Pb data has been made using the measured $^{238}U/^{206}Pb$ and $^{207}Pb/^{206}Pb$ ratios following Tera and Wasserburg (1972) as outlined in Williams (1998).

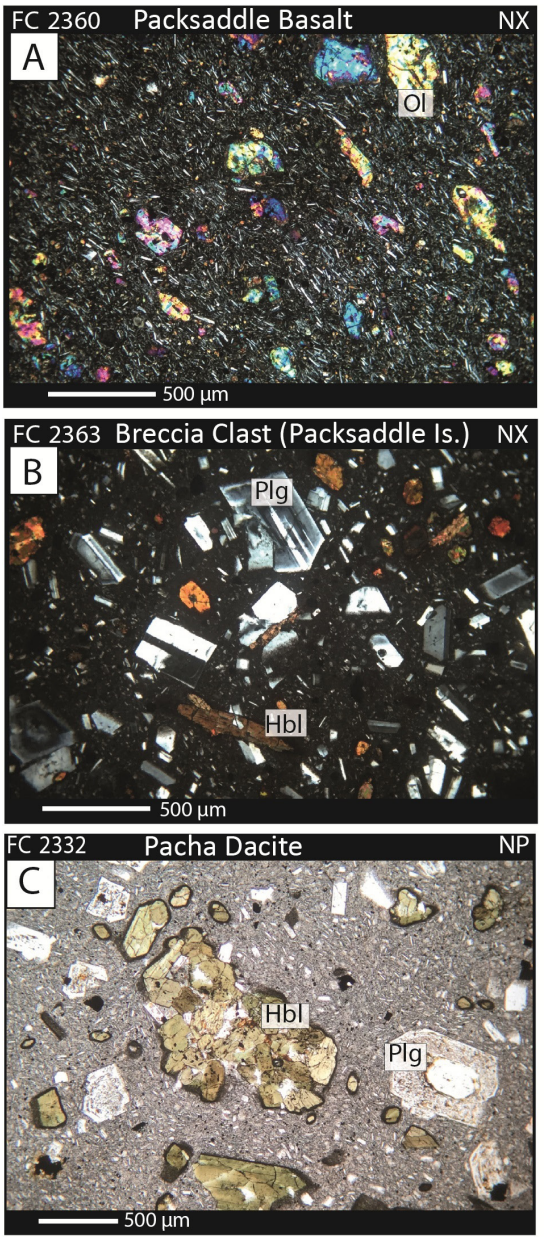

FIG. 4. Typical petrography of the Packsaddle Volcanic Complex. **A.** Olivine-basalt, Packsaddle Island. **B.** Dacite clast from the basal breccia, Packsaddle Island. **C.** Hornblende-dacite, Pacha Island. Hbl: Hornblende; Plg: Plagioclase. NX: Crossed nicols; NP: Parallel nicols. See figure 1 for sample locations.

4.2. Geochemistry of the PVC

New geochemical data are reported from nine samples of basalts, andesites, dacites and intrusive from Packsaddle Island, Pacha Island, and Hardy Peninsula (Figs. 5 and 6; Table 1). The results are combined with previously published data from the PVC (Puig *et al.*, 1984; Ramírez de Arellano *et al.*, 2021) and the integrated datasets are compared with data for three Neogene igneous suites from the Patagonia domain to the north of the studied area, as defined by Ramírez de Arellano *et al.* (2021).

The olivine basalts from Packsaddle Island show alkaline to subalkaline affinities (Fig. 5A) in a narrow range of SiO_2 (47.2-49.5 wt.%), with high Mg# (~66.5%), Ni ~ 160 ppm (up to 220 ppm), Cr ~ 320 ppm (up to 380 ppm), and high concentration of TiO_2 and P_2O_5 (>1.5 wt.% and >0.3 wt.%, respectively). Three samples reported by Puig *et al.* (1984) and two samples reported by Ramírez de Arellano *et al.* (2021) follow the same trends. In a multi-element diagram normalized to Primitive Mantle (Fig. 6) these rocks show an enrichment of large ion lithophile elements (LILE). However, the preferential enrichment of LILE over high field strength elements (HFSE), typical of arc magmas, is not pronounced, as also indicated by the low Ba/Nb ratios (<30, except one at 47; Fig. 5F). These rocks show positive anomalies of Ti and P compared to heavy rare earth elements (HREE) like Gd or Tb (Fig. 6). Only a subtle Pb positive anomaly is observed (Ce/Pb >3; Fig. 6). In terms of REE, these rocks also present a preferential enrichment of light rare earth elements (LREE) over HREE, with no Eu anomaly (Fig. 6). The $(La/Yb)_n$ and $(Dy/Yb)_n$ ratios are moderately high (~9 and ~1.3, respectively), exhibiting a narrow variability. In comparison with common arc-related magmas (*e.g.,* South Patagonian Batholith and Southern Volcanic Zone of the Andes; Hervé *et al.*, 2007; Hickey-Vargas *et al.* 2016), these rocks have low Rb/Ba, Ba/Nb (<0.04 and <30, respectively; Fig. 5D, F), and high Nb/U (>13.7), Sr/Y (>38; Fig. 5C), Ce/Pb (>3) and La/Th (>6.4; Fig. 5E) ratios. These element ratios indicate a signature intermediate between arc and intraplate (OIB-like).

The dacites from Pacha Island share a common signature with the dacite clasts from the pyroclastic breccias at Packsaddle Island and the andesites and dacites from Hardy Peninsula reported by Puig *et al.* (1984). As shown in figure 5A, these rocks display a subalkaline character, well below the line separating alkaline from subalkaline fields, covering a compositional range of 61 to 65 wt.% SiO_2, 18.2 to 16.5 wt.% Al_2O_3, TiO_2 <0.85 wt.%, P_2O_5 <0.25 wt.%, and relatively high Mg# (*e.g.,* 57 at 57.3 wt.% SiO_2; 44 at 63 wt.% SiO_2). Notably, these rocks

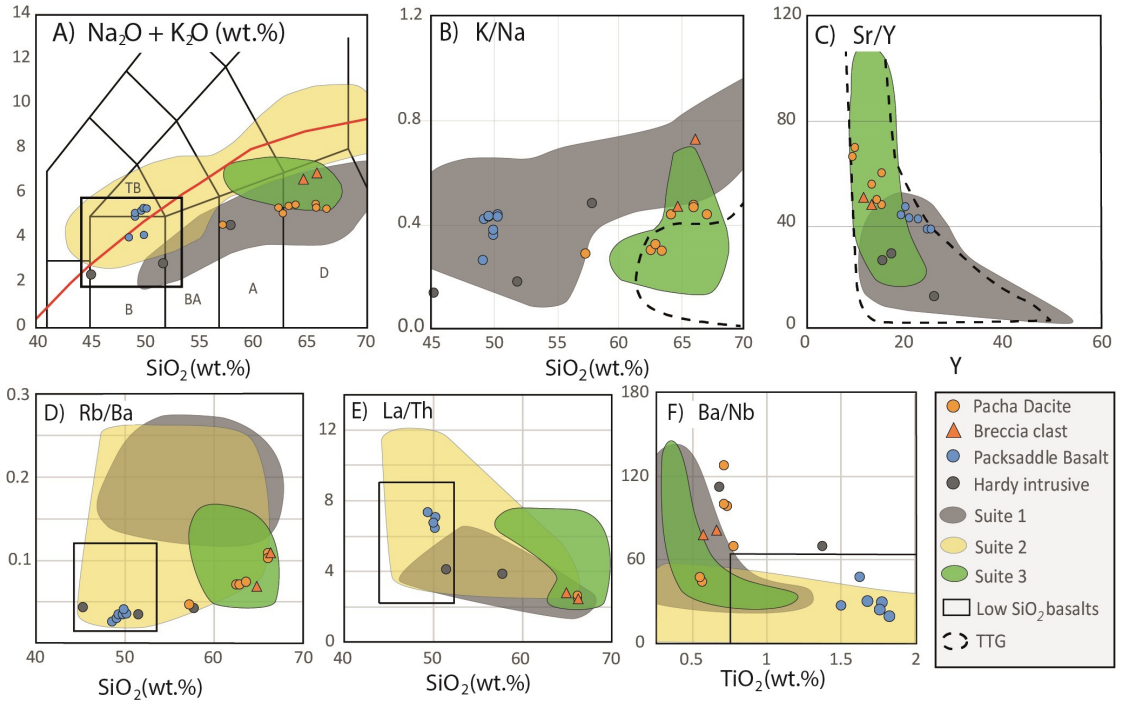

FIG. 5. Main geochemical features of Packsaddle Basalts (blue circles), Pacha Dacites (orange circles), plus two breccia clasts from Packsaddle Island (orange tringles), and Hardy Peninsula intrusives. **A.** TAS diagram with alkaline-subalkaline limit (red line) after Irvine and Baragar (1971). (TB: trachybasalt, B: basalt, BA: basaltic andesite, A: andesite, and D: dacite.) **B.** K/Na ratios vs. silica. **C.** Sr/Y vs. Y. **D** and **E** show Rb/Ba and La/Th ratios vs. silica. **F.** Ba/Nb ratios vs. TiO_2 (high values correlate with a HFSE negative anomaly; low TiO_2 denotes negative Ti anomaly relative to HREE; see also figure 6). Suites 1, 2, and 3 represent the Neogene Patagonian magmatism north of 53° S (Ramírez de Arellano *et al.*, 2021). Suite 1 (grey area) corresponds to the Neogene calc-alkaline South Patagonian Batholith, exemplifying typical Andean magmatism; Suite 2 (yellow area) includes slightly alkaline rocks formed immediately before the opening of the slab window; Suite 3 (green area) corresponds volcanic to subvolcanic high Sr/Y andesites coeval with Suite 2. Note the similarities of Packsaddle Basalts with Suite 2 and Pacha Dacites with Suite 3, as well as between the Packsaddle Basalts and the low-silica primary basalts (black frame rectangles) from the global compilation of subduction-related primary magmas by Schmidt and Yagoutz (2017). Conversely, the Pacha Dacites correlate well with the Archean TTG Suite (dashed black lines in panels B and C), as an ancient analogue of hot subduction magmatism.

exhibit low K/Na ratios (<0.5) comparable to the Archean TTG suites (Fig. 5B). There is a clear arc-like trace element signature, namely a preferential enrichment of LILE over HFSE with a marked Nb-Ta negative anomaly, high Rb/Ba ratios (>0.05), and a well-marked Pb positive anomaly (Ce/Pb <2.2), as shown in the multi-element diagram normalized to Primitive Mantle (Fig. 6). In terms of the REE, these rocks are preferentially enriched in LREE over HREE, with a relatively high $(La/Yb)_n$ and moderated $(Dy/Yb)_n$ ratios (~11 and ~1.2, respectively), like the olivine basalts from Packsaddle Island, and a notable absence of Eu anomalies (Fig. 6). As mentioned, the most remarkable feature of these rocks is their high Sr/Y ratios (>40; Fig. 5C), due to their relatively high Sr contents (>570 ppm). Another feature of these rocks is the Th and U higher than K and Rb when normalized to Primitive Mantle (Fig. 6).

The signatures of the micro-gabbro (FC2349) from Hardy Peninsula (51.6 wt.% SiO_2; Mg# 65) and the plutonic rocks from the same locality, differ from those of the Pacha Dacites and Packsaddle Basalts (Fig. 6). They display a subalkaline character and trace element ratios (*e.g.,* Ba/Nb >70; Sr/Y <40) similar to those observed in most of the plutons from the Patagonian Batholith and volcanic products of the Southern Volcanic Zone of the Andes (Hervé *et al.*, 2007; Hickey-Vargas *et al.*, 2016).

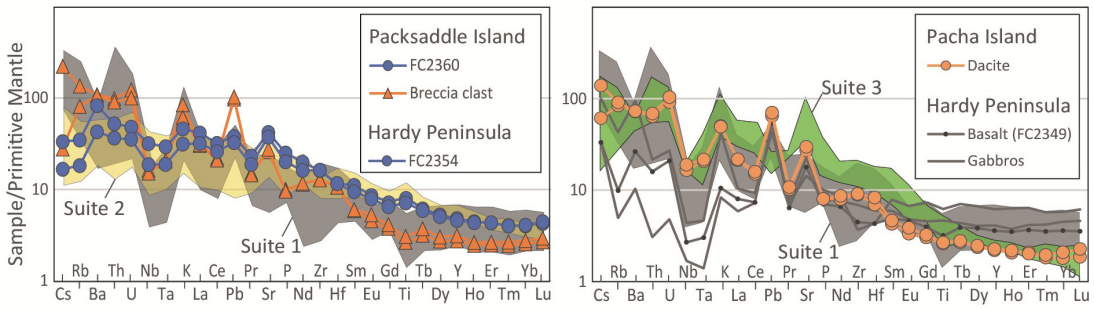

FIG. 6. Multi-element (spider) diagrams normalized to Primitive Mantle (Palme and O'Neill, 2014) for representative samples from Packsaddle and Pacha islands and Hardy Peninsula. Fields are shown for Neogene Patagonian Suites 1 (grey), 2 (yellow), and 3 (green), as in figure 5.

4.3. U-Pb zircon geochronology

Zircons from a hornblende vitreous-crystalline dacite tuff fragment within the lower volcanic breccia of Packsaddle Island were analysed. The sample (FC2362-A) consists of crystals (30%; <1mm), mainly plagioclase, hornblende, and minor biotite, in a vitreous to crystalline matrix (70%). The breccia is intruded by a basaltic sill and is thus expected to record the age of explosive andesite-dacite volcanism prior to the emplacement of the basalts. Twenty-two zircons were analysed by SHRIMP U-Pb (Table 2). Twenty-one grains yield a mean age of 20.5±0.2 Ma (Fig. 7). One zircon yielded an age of *ca.* 104 Ma and is presumed to be an inherited xenocryst.

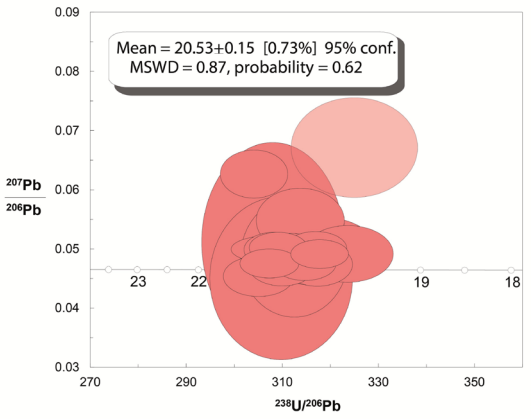

FIG. 7. Concordia plot of zircon U-Pb SHRIMP data for sample FC2362-A, a dacitic tuff clast from the basal breccia on Packsaddle Island. The pale shaded ellipse is for analysis 22.1 (not used in the age calculation). MSWD: mean square weighted deviation.

4.4. Isotope chemistry of the PVC

Sr and Nd isotope compositions of five samples were determined (Fig. 8; Table 3): two olivine basalts and the dated dacite tuff clast from Packsaddle Island, a dacite from Pacha Island, and a micro-gabbro from Hardy Peninsula.

The two basalts yield indistinguishable initial $^{87}Sr/^{86}Sr$ (0.70392 and 0.70387) and $^{143}Nd/^{144}Nd$ (0.512870 and 0.512878; εNd_i = +5.0/5.2) ratios. The micro-gabbro (FC2349) from Hardy Peninsula

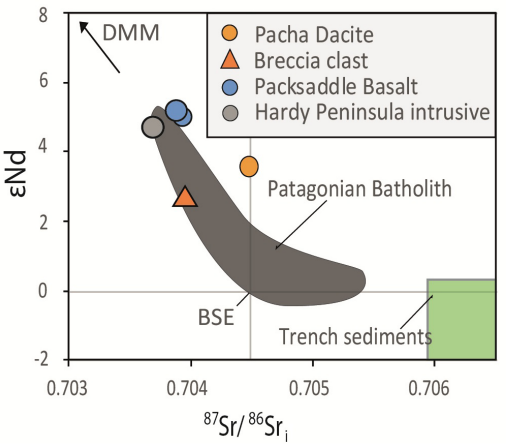

FIG. 8. εNd vs. $^{87}Sr/^{86}Sr$ diagram for the Pacha Dacites and Packsaddle Basalts. The grey field represents the Patagonian Batholith (Hervé *et al.*, 2007), which corresponds to Suite 1 (see figures 5 and 6). Isotopic composition from Depleted MORB Mantle (DMM) according to Salters and Stracke (2004). Trench sediments after Kilian and Behrmann (2003). BSE: Bulk Silicate Earth isotopic composition at present.

TABLE 3. ISOTOPIC GEOCHEMISTRY OF THE PACKSADDLE VOLCANIC COMPLEX. CLAST (FC2362-A).

Sample	Rock type	Sm [ppm]	Nd [ppm]	$^{147}Sm/^{144}Nd$	$^{143}Nd/^{144}Nd$	$(^{143}Nd/^{144}Nd)_i$ (t=20 Ma)*	εNd	Rb [ppm]	Sr [ppm]	Rb/Sr	$^{87}Rb/^{86}Sr$	$^{87}Sr/^{86}Sr$	$(^{87}Sr/^{86}Sr)_i$ (t=20 Ma)*
Packsaddle Island													
FC2360	Ol-basalt	4.81	26.7	0.108918	0.512884	0.512870	5.0	21	923	0.02275	0.06580	0.70394	0.70392
11TU-5801	Basalt	4.78	26.1	0.110727	0.512893	0.512878	5.2	18	873	0.02062	0.05963	0.70389	0.70387
FC2362-A	Dacite clast	2.55	15.3	0.100763	0.512762	0.512749	2.7	82	570	0.14386	0.41608	0.70408	0.70396
Pacha Island													
FC2330	Dacite	1.86	10.7	0.105096	0.512812	0.512798	3.6	51	598	0.08528	0.24667	0.70453	0.70446
Hardy peninsula													
FC2349	Micro-gabbro	2.13	8.9	0.145512	0.512870	0.512851	4.7	6	393	0.01527	0.04415	0.70371	0.70369

*The initial ratios were calculated using the zircon age of ~20 Ma from the dacite tuff.

has a radiogenic signature similar to the Packsaddle basalts ($^{87}Sr/^{86}Sr_i$=0.70369; εNd_i=+4.7). The dated tuff clast from the lower breccia on Packsaddle Island shows a similar initial $^{87}Sr/^{86}Sr$ (0.70396) and a lower initial $^{143}Nd/^{144}Nd$ (0.512749, εNd_i=+2.7) compared to the basalts. The Pacha Island dacite has the highest initial $^{87}Sr/^{86}Sr$ (0.70446), but a comparable $^{143}Nd/^{144}Nd_i$=0.512798 (εNd_i=+3.6) to the dated dacitic clast.

5. Discussion

5.1. Petrogenesis of the Packsaddle Basalts

The low SiO_2 concentration of these rocks (<50 wt.%), together with their high Mg# (up to 67), high concentration of Ni (up to 220 ppm) and Cr (up to 380 ppm), and their uniform Sr and Nd isotope compositions, suggests a mantle source of magmas with little chemical differentiation or crustal assimilation. Their transitional geochemistry between alkaline and subalkaline affinities suggests low degrees of melting, while their high FeO/MgO ratios, at the boundary between tholeiitic and calc-alkaline series, suggest less oxidizing conditions than for the typical calc-alkaline magmas of the Patagonian Batholith and lavas from the Southern Volcanic Zone (Hervé *et al.*, 2007; Hickey-Vargas *et al.*, 2016). Their trace element signatures, with transition from arc-related to intraplate (OIB-like) affinities, suggest important variation either in the mantle source or in the thermodynamic conditions that generated these magmas compared with "Andean" conditions.

Upper Miocene (<8 Ma) OIB-like basalts along Patagonian and Antarctic Peninsula margins coincide spatially with the current slab windows associated with the Chile Ridge (Nazca-Antarctica Ridge) and the Antarctic-Phoenix Ridge, respectively (*e.g.,* Gorring and Kay, 2001; D'Orazio *et al.*, 2004; Hole *et al.*, 2021, 2023). Hole *et al.* (2023) proposed that they were generated from a source dominated by pyroxenites instead of the peridotites of typical arc mantle sources. In this model, the transitional magmas of the Packsaddle Basalts could have been generated from an intermediate source, due to a shifting of the locus of mantle melting or due to erosion of lithospheric mantle as proposed by Turner *et al.* (2017). Their LILE patterns (*e.g.,* with Cs and Rb less enriched than Ba and K and low Rb/Ba; see figures 5 and 6) would support a mixture between a subduction-like and an OIB-like sources. Nevertheless, other geochemical features of the Packsaddle Basalts require explanation. The high concentration of REE, consistently with relative enrichment in alkalis, supports lower degrees of melting than for typical calc-alkaline rocks. Likewise, the less oxidizing conditions suggested by the high Feo/MgO ratios would be consistent with the low concentration of fluid-mobile elements such as Pb and U compared to LREE (see figure 6), indicating a lower flux of fluid from the slab. Finally, the high concentration of HFSE, mainly Nb, Ta, and TiO_2, compared to LILE (as shown by the low Ba/Nb ratios; see figures 5 and 6), suggests decreasing stability of refractory phases such as rutile, which is thought to be the main carrier of these elements to the lower mantle.

Considering that rutile is stable at pressures higher than ~1.5 GPa and temperatures lower than ~1,000 °C (for a system with 2% H_2O; Xiong *et al.*, 2005; Skora and Blundy, 2010), its instability could be related to warmer conditions during slab dehydration (see figure 9) or melting of a lithospheric mantle previously enriched. These conditions could indicate an abnormal thermal regime induced by the presence of the NAZ-PHO slab window immediately to the north of this region. Similar conditions in the context of Chile Ridge subduction allowed melt extraction at intermediate degrees of mantle melting (Ramírez de Arellano *et al.*, 2021).

The isotopic composition of Packsaddle Basalts resembles the less contaminated products of the Patagonian Batholith ($^{87}Sr/^{86}Sr_i \approx 0.7038$; $\varepsilon Nd_i \approx 5.0$; Hervé *et al.*, 2007), confirming minimal crustal anataxis and implying rapid ascent (see figure 8). The isotopic difference with respect to a depleted MORB mantle, calculated at 20 Ma ($^{87}Sr/^{86}Sr_i=0.70263$; $^{143}Nd/^{144}Nd_i=0.51313$; Salters and Stracke, 2004) can be attributed to fluid-melt interactions with the mantle wedge or to ancient enriched domains in the lithospheric mantle.

5.2. Petrogenesis of the Pacha Dacites

The Pacha Dacites exhibit a clear arc-related trace element signature with a notable enrichment of LILE over HFSE, a negative anomaly of Ti, and a positive anomaly of Pb (see figure 6). However, they also present certain features that distinguish them from typical arc magmas, namely low K/Na ratios, relatively high Mg# (with respect to SiO_2 concentration), relatively high Sr/Y and La/Yb ratios, absence of Eu anomaly, and low HREE concentrations (see figures 5 and 6). The high Sr/Y together with the low K/Na ratios and the absence of Eu anomaly can be attributed to a lack of fractionation or delayed plagioclase crystallization, which is rare for such evolved rock compositions. Experimental and theoretical studies show that dissolved H^2O in the magma, and pressure, significantly influence plagioclase stability and crystallization order in mafic-intermediate systems (*e.g.,* Goldsmith, 1982; Gaetani *et al.*, 1993). Given the calc-alkaline character and the abundance of hornblende in the Pacha Dacites, the parent magmas must have had high water contents. It is hard to make a precise estimate of the pressure: high-pressure magma differentiation is characterized by amphibole or garnet, either as a fractionated phase or as a stable phase in the residue (*e.g.,* Davidson *et al.*, 2007; Gao *et al.*, 2023). These two phases have high HREE partition coefficients ($K_D>1$): amphibole has similar K_D for all HREE from Dy to Yb, whereas garnet has $K_D(Yb)>>K_D(Dy)>1$ (ibid.). The high La/Yb ratios observed in the Pacha Dacites could indicate the effect of both minerals. Nevertheless, despite the low concentration of HREE (only two to three times that of Primitive Mantle), the relatively low Dy/Yb ratios (see figure 6) argue in favour of amphibole fractionation. The relatively high Mg# at a given SiO_2 compared to a typical calc-alkaline series may also be explained by amphibole fractionation. Because of its low SiO_2 concentration, fractionation of amphibole would increase SiO_2 in the residual melt more efficiently than clinopyroxene (the other ferromagnesian candidate). The low La/Th ratios (indicative of high Th concentration; see figure 5) observed in the Pacha Dacites, together with the slightly less radiogenic Sr isotopic signature, suggest some participation of crustal material, possibly from sediment subduction, during melting in the mantle wedge (see figure 8).

Partial melting of mafic rocks from the slab or the sub-arc crust has been invoked to explain the genesis of high Sr/Y rocks (*e.g.,* Defant and Drummond, 1990; Moyen, 2009; Yang *et al.*, 2020; Zhang *et al.*, 2021; Wang *et al.*, 2022; Xu and Chen, 2023). Conversely, high-pressure experiments have shown that amphibole fractionation and delayed plagioclase crystallization can also generate high Sr/Y melts (Müntener *et al.*, 2001; Davidson *et al.*, 2007; Alonso-Perez *et al.*, 2009; Nandedkar *et al.,* 2014, 2016; Gao *et al.*, 2023). It has also been proposed that the parental magmas for these suites could be mantle-derived high-Mg andesites (HMA) resulting from re-equilibration of basaltic melts in the upper section of the mantle wedge (Schmidt and Jagoutz, 2017).

Despite the sparse sampling, the absence of mafic (basaltic) members with the trace-element characteristics of the Pacha Dacites, combined with the relative homogeneity of trace-element ratios for andesites to dacites (60-65 wt.% SiO_2), suggests that their parental melts were intermediate, probably high-Mg andesites. Because there is no evidence for garnet involvement in the evolution of the Pacha Dacites, we favour a deep fractional-crystallization model from an intermediate parent magma, characterized by amphibole fractionation with delayed plagioclase crystallization. Differentiation may have been accompanied by some mid- to lower-

crustal assimilation to account for the elevated Th concentrations and isotopic signature of the Pacha Dacites (see figures 5, 6, and 8). The interpreted deep fractional-crystallization process means that upper-crustal contamination is unlikely. Mantle-derived contamination, either via metasomatism with subducted sediments or melting of a heterogeneous lithospheric mantle, cannot be ruled out. Testing in detail any of these hypotheses falls outside the scope of this work, and a detailed isotopic study would be required.

5.3. Time, spatial and geochemical relationship

The available time constraints and the lack of any evidence for a mixing trend between the signatures from Packsaddle Basalts and Pacha Dacites suggest two discrete volcanic events rather than coeval bimodal magmatism or a continuous variation in the melting mechanism: we rather propose intermediate volcanism dominated by high Sr/Y andesites and dacites, later followed by olivine-bearing basaltic magmas. This is consistent with the new U-Pb zircon age (20.5±0.2 Ma) and the previous K-Ar dating of 21±0.2 Ma for a dacite and 18.5±0.2 Ma for the olivine basalts (Puig *et al.*, 1984). The distinctive geochemical characteristics of the Pacha Dacites are also observed in the breccia clast from Packsaddle Island and the andesite-dacites from Hardy Peninsula reported by Suárez *et al.* (1985). In contrast, the micro-gabbro (FC2349) and associated plutonic rocks from Hardy Peninsula do not match either the Pacha Dacites or the Packsaddle Basalts, and it could correspond to an even earlier magmatic event. No field relationships have been observed among these three units aside from the breccia on Packsaddle Island.

Given the age established, a causal relationship between PVC magmatism and the subduction of the NAZ-PHO spreading ridge is feasible. Tectonic reconstruction shows the correspondence between the location of the PVC and the slab window generated by the NAZ-PHO ridge (Breitsprecher and Thorkelson, 2009; Eagle and Jokat, 2014; Eagles and Scott, 2014) (Fig. 2). Despite the fast motion (>10 km/Myr) of the Nazca and Phoenix plates with respect to the South American plate at 20 Ma, the low relative velocity between these two oceanic plates generated a narrow E-W oriented slab window below the Fuegian domain (Scotia Plate) to the north of the PVC (Fig. 2 left panel; Fig. 9). At that time, the high Sr/Y intermediate magmas were erupted above the slab corresponding to the Phoenix Plate. Between 20 and 16 Ma, subduction of the Nazca-Phoenix-Antarctic triple junction widened the slab window, ultimately leaving the PVC above it. This implies that, during emplacement of the Packsaddle Basalts, the last fluids and melts from the Phoenix Plate were injected into the mantle wedge at sub-arc depths. Because subduction was highly oblique, the northern edge of the Phoenix Plate moved nearly parallel to the margin beneath the arc, supplying the subduction component during that interval (see figures 2 and 9). This was likely accompanied by an anomalously high thermal gradient caused by the continuous presence of the slab window immediately to the north.

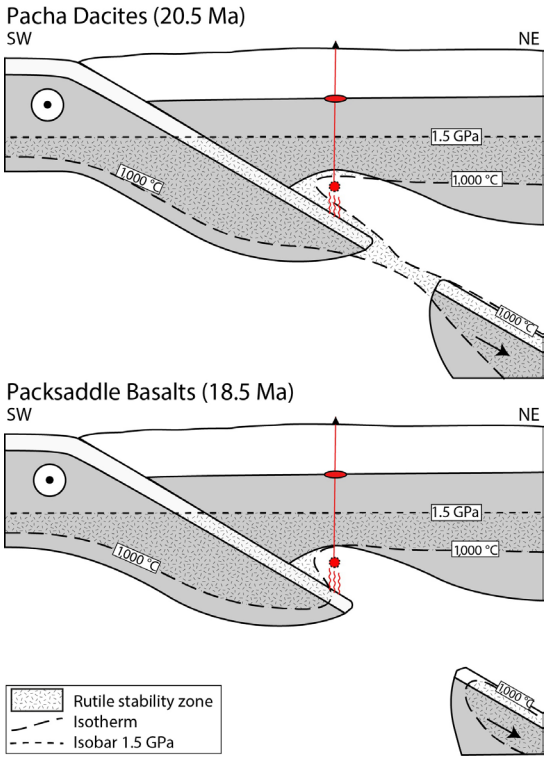

FIG. 9. Schematic subduction profile along a SW-NE section perpendicular to the margin in the Fuegian domain, where Packsaddle Island is located, at the time of formation of the PVC. Because the Phoenix-Scotia convergence vector is almost parallel to the margin (see figure 2), the Phoenix slab appears effectively stationary beneath the arc, whereas the Nazca slab is migrating slowly northward. Before the opening of the slab window beneath the arc, the 1,000 °C isotherm splits toward both slabs, promoting rutile destabilization and the transfer of Na-Ta into the mantle wedge.

Comparison with magmatic suites produced during subduction of the Chile Ridge in the Patagonian domain north of this region reveals striking similarities. Five suites have been recognized before, during, and after opening of the Chile Ridge slab window (Ramírez de Arellano *et al.*, 2021). Three of these suites are considered here for discussion. The first suite is "normal" medium-K calc-alkaline, recorded in the batholith and satellite plutons (Hervé *et al.*, 2007; Ramírez de Arellano *et al.*, 2012). The second suite is "transitional" magmatism that becomes progressively richer in alkalis as the slab window approaches, marking a shift from typical arc signatures toward intraplate-like compositions (*e.g.,* Gorring *et al.*, 1997; D'Orazio *et al.*, 2004; Guivel *et al.*, 2006; Corbella and Lara, 2008). Coevally, the third suite corresponds to volcanic and subvolcanic andesites with high Sr/Y ratios, previously reported along the arc domain (Kay *et al.*, 1993; Ramos *et al.*, 2004). These three suites correlate well with the PVC sub-units (see figures 5 and 6).

The plutonic rocks from Hardy Peninsula can be interpreted as a mafic member of the Palaeogene Seno de Año Nuevo Group defined by Suárez *et al.* (1985). The micro-gabbro sample FC2349 from Hardy Peninsula also exhibits a signature consistent with "normal" medium-K calc-alkaline Suite 1. However, in the absence of stratigraphic or geochronological constraints, its origin remains ambiguous: it could belong to a younger Neogene volcanic unit or represent a Palaeogene dike crosscutting the folded Jurassic to Cretaceous successions. If it is a Neogene volcanic unit, it would constitute the third (and oldest) member of the PVC.

The chemistry of the Pacha Dacites conforms to the calc-alkaline series, but with characteristic high Sr/Y, low K/Na ratios (Fig. 5B, C), relatively high Mg# for a given SiO_2, and low concentrations of HREE (Dy to Lu; see figure 6). These features closely resemble Suite 3 of the Patagonian domain (Figs. 5 and 6). On the other hand, the transitional signatures of the Packsaddle Basalts fit well with Suite 2 (Figs. 5 and 6). Their alkaline to subalkaline character, with FeO/MgO ratios near the tholeiitic-calc-alkaline boundary and transitional trace-element ratios, intermediate between arc-related and intraplate (OIB-like) signatures, are also characteristic of subduction-related primary melts termed "low-SiO_2 basalts" (Schmidt and Jagoutz, 2017; see figure 5).

One crucial observation is that, whereas in the Patagonian domain, associated with subduction of the Chile Ridge, the transitional magmatism occurred coevally with the high Sr/Y andesites, in the Fuegian domain, associated with subduction of the NAZ-PHO ridge, field observations and available geochronology indicate that the Sr/Y andesite-dacites occurred slightly before the transitional basaltic magmatism. Nevertheless, in both cases a more detailed geochronological study is required to precisely determine the lifespans and the relative timing of the magmatic episodes.

5.4. Bimodal arc-like magmatism related to oceanic ridge subduction

Several features of the Pacha Dacites and Packsaddle Basalts can be attributed to the subduction of the NAZ-PHO ridge and the approach of the related slab window to the sub-arc depths. Despite the differences between them, their similar REE patterns (relatively high La/Yb and low Dy/Yb) suggest that their primary melts formed at comparable depths, above the garnet-lherzolite stability field. Very little interaction with the continental crust for the Packsaddle Basalts is shown by their primitive geochemical and isotopic features. In the case of the Pacha Dacites, their chemistry implies deep-seated fractionation. Therefore, their isotopic signature can be attributed to minor lower crustal contamination or source contamination. Low interaction with the mid to upper continental crust and therefore a rapid ascent is suggested in both cases, which can be attributed to an extensional regime triggered by the NAZ-PHO spreading ridge at sub-arc depths (Fig. 9).

The contrasting alkalinity of these two PVC units, together with their different concentrations of REE, implies substantially different degrees of mantle melting. The subalkaline magmatism of the Pacha Dacites is typically associated with high degrees of mantle melting, due to metasomatism of the mantle wedge, and is consistent with high concentrations of fluid mobile elements like U and Pb. An alkaline magma series, such as the Packsaddle Basalts, implies lower degrees of partial melting, concentrating alkalis and other incompatible elements like REE, but lower U and Pb anomalies. The lower melting degrees inferred for the Packsaddle Basalts could be attributed to a rise of the mantle solidus caused

by a progressively decreasing flux of slab-derived fluids and melts. This interpretation is consistent with the tectonic setting, given that the subducted Phoenix Plate supplied its final fluid-melts prior to the opening of the NAZ-PHO slab window and the cessation of arc magmatism (see figure 9).

Finally, the trace-element signature of the Packsaddle Basalts, notably the attenuated negative HFSE anomaly relative to LILE, as shown, for instance, by the low Ba/Nb ratios (<30), suggests an anomalously high thermal gradient. HFSE enrichment is commonly attributed to mantle re-fertilization at intraplate mantle sources, where elevated temperatures destabilize rutile (*e.g.,* Zheng, 2019). The Packsaddle Basalts chemistry suggests that Nb and Ta were released into the mantle wedge while fluids/melts were still acting as metasomatic agents at sub-arc depths. This may reflect early destabilization of refractory phases, like rutile or clinohumite, in metasomatized domains at the slab-mantle interface. Enhanced heat flow from a nearby slab window, as observed in the Chile Ridge case (*e.g.,* Sanhueza *et al.*, 2023), could raise temperatures at the slab-mantle interface above typical values (*e.g.,* Syracuse *et al.*, 2010), allowing metasomatism to proceed under conditions where rutile is not stable (pressures ≲1.5 GPa or temperatures ≲1,000 °C; Xiong *et al.*, 2005; Skora and Blundy, 2010; see figure 9). Further detailed study of these magmas would improve constraints on thermodynamic conditions and metasomatic processes from sub-arc to greater depths.272

6. Conclusions

This study documents a bimodal magmatic association in the Packsaddle Volcanic Complex (PVC) through the integration of U-Pb zircon geochronology, whole-rock geochemistry, and Sr-Nd isotopic data. U-Pb dating of a dacitic clast (20.5±0.2 Ma) confirms the Early Miocene (Aquitanian-Burdigalian) age of high Sr/Y intermediate magmatism. Field observations demonstrate that this magmatism preceded mildly alkaline basaltic activity, indicating a temporal evolution rather than coeval bimodal volcanism.

The Pacha Dacites in the PVC show calc-alkaline signatures with high Sr/Y ratios and low HREE contents, consistent with deep differentiation of hydrous intermediate magmas dominated by amphibole fractionation. In contrast, the Packsaddle Basalts represent relatively Primitive Mantle-derived melts, characterized by low SiO_2, high Mg#, and transitional arc to intraplate geochemical affinities. Their Sr-Nd isotopic compositions indicate limited crustal assimilation. These contrasting magmatic suites reflect a shift in the thermal and geodynamic regime of the subduction zone. Early intermediate calc-alkaline magmatism formed under conditions with strong slab-derived input, whereas later basaltic magmatism records reduced slab influence, lower degrees of melting, and higher thermal gradients.

We interpret these magmatic suites as the result of ridge subduction and slab window development, which modified the thermal structure of the mantle wedge and resulted in a shift from arc-like to more intraplate-like compositions.

Acknowledgements

The Packsaddle Island is one of more than hundred Geosites identified by the Sociedad Geológica de Chile. This program was leaded by Pancho Hervé during its participation as Director, to identify and valorise the geological heritage of Chile. The new data reported here were funded by FONDECYT project N°1211906 (Chile). The authors thank the students and colleagues involved in the field seasons for their constructive discussion. The authors also thank Capitán H. Cárdenas and the crew of Huracán. Constructive comments from M. Hole and an anonymous reviewer improved this manuscript. B. Pankhurst, as Guest Editor, and D. Bertin, as Editor-in-Chief, further enhanced it with their recommendations.

References

Alonso-Pérez, R.; Müntener, O.; Ulmer, P. 2009. Igneous garnet and amphibole fractionation in the roots of island arcs: experimental constraints on andesitic liquids. Contributions to Mineralogy and Petrology 157 (4): 541-558. https://doi.org/10.1007/s00410-008-0351-8

Black, L.; Kamo, S.; Allen, C.M.; Aleinikoff, J.; Davis, D.; Korsch, R.; Foudoulis, C. 2003. TEMORA 1: A new zircon standard for Phanerozoic U-Pb geochronology. Chemical Geology 200: 155-170. https://doi.org/10.1016/s0009-2541(03)00165-7

Breitsprecher, K.; Thorkelson, D.J. 2009. Neogene kinematic history of Nazca-Antarctic-Phoenix slab windows beneath Patagonia and the Antarctic Peninsula. Tectonophysics 464 (1-4): 10-20. https://doi.org/10.1016/j.tecto.2008.02.013

Calderón, M.; Fildani, A.; Hervé, F.; Fanning, C.M.; Weislogel, A.; Cordani, U. 2007. Late Jurassic bimodal magmatism in the northern sea-floor remnant of the Rocas Verdes basin, southern Patagonian Andes. Journal of the Geological Society 164 (5): 1011-1022. https://doi.org/10.1144/0016-76492006-102

Cande, S.C.; Leslie, R.B. 1986. Late Cenozoic tectonics of the Southern Chile Trench. Journal of Geophysical Research, Solid Earth 91 (B1): 471-496. https://doi.org/10.1029/jb091ib01p00471

Corbella, H.; Lara, L.E. 2008. Late Cenozoic Quaternary Volcanism in Patagonia and Tierra del Fuego. *In* The Late Cenozoic of Patagonia and Tierra del Fuego (Rabassa, J.; editor). Developments in Quaternary Sciences 11: 95-119. https://doi.org/10.1016/s1571-0866(07)10006-3

D'Orazio, M.; Innocent, F.; Manetti, P.; Haller, M.J. 2004. Cenozoic back-arc magmatism of the southern extra-Andean Patagonia (44°30'-52° S): A review of geochemical data and geodynamic interpretations. Revista de la Asociación Geológica Argentina 59 (4): 525-538.

Dalziel, I.; De Wit, M.; Palmer, K. 1974. Fossil marginal basin in the southern Andes. Nature 250: 291-294. https://doi.org/10.1038/250291a0

Davidson, J.; Turner, S.; Handley, H.; Macpherson, C.; Dosseto, A. 2007. Amphibole "sponge" in arc crust? Geology 35 (9): 787-790. https://doi.org/10.1130/g23637a.1

Defant, M.; Drummond, M. 1990. Derivation of some modern arc magmas by melting of young subducted lithosphere. Nature 347: 662-665. https://doi.org/10.1038/347662a0

Eagles, G.; Jokat, W. 2014. Tectonic reconstructions for paleobathymetry in Drake Passage. Tectonophysics 611: 28-50. https://doi.org/10.1016/j.tecto.2013.11.021

Eagles, G.; Scott, B.G.C. 2014. Plate convergence west of Patagonia and the Antarctic Peninsula since 61 Ma. Global and Planetary Change 123 (B): 189-198. https://doi.org/10.1016/j.gloplacha.2014.08.002

Espinoza, F.; Morata, D.; Polve, M.; Lagabrielle, Y.; Maury, R.; De la Rupelle, A.; Guivel, C.; Cotten, J.; Bellon, H.; Suárez, M. 2010. Middle Miocene calc-alkaline volcanism in Central Patagonia (47° S): petrogenesis and implications for slab dynamics. Andean Geology 37 (2): 300-328. https://doi.org/10.5027/andgeov37n2-a03

Gaetani, G.; Grove, T.; Bryan, W. 1993. The influence of water on the petrogenesis of subductionrelated igneous rocks. Nature 365: 332-334. https://doi.org/10.1038/365332a0

Gao, Y.; O'Neill, H.S.C.; Mavrogenes, J.A. 2023. Garnet versus amphibole: Implications for magmatic differentiation and slab melting. Geology 52 (2): 125-129. https://doi.org/10.1130/g51637.1

Goldsmith, J. 1982. Plagioclase stability at elevated temperatures and water pressures. American Mineralogist 67 (7-8): 653-675.

Gómez-Tuena, A.; Cavazos-Tovar, J.G.; Parolari, M.; Straub, S.M.; Espinasa-Pereña, R. 2018. Geochronological and geochemical evidence of continental crust 'relamination' in the origin of intermediate arc magmas. Lithos 322: 52-66. https://doi.org/10.1016/j.lithos.2018.10.005

Gorring, M.L.; Kay, S.M. 2001. Mantle processes and sources of Neogene slab window magmas from Southern Patagonia, Argentina. Journal of Petrology 42 (6): 1067-1094. https://doi.org/10.1093/petrology/42.6.1067

Gorring, M.L.; Kay, S.M.; Zeitler, P.K.; Ramos, V.A.; Rubiolo, D.; Fernández, M.I.; Panza, J.L. 1997. Neogene Patagonian plateau lavas: Continental magmas associated with ridge collision at the Chile Triple Junction. Tectonics 16 (1): 1-17. https://doi.org/10.1029/96tc03368

Guivel, C.; Morata, D.; Pelleter, E.; Espinoza, F.; Maury, R.C.; Lagabrielle, Y.; Polvé, M.; Bellon, H.; Cotten, J.; Benoit, M.; Suárez, M.; De la Cruz, R. 2006. Miocene to Late Quaternary Patagonian basalts (46-47°S): Geochronometric and geochemical evidence for slab tearing due to active spreading ridge subduction. Journal of Volcanology and Geothermal Research 149 (3-4): 346-370. https://doi.org/10.1016/j.jvolgeores.2005.09.002

Hervé, F.; Pankhurst, R.J.; Fanning, C.M.; Calderón, M.; Yaxley, G.M. 2007. The South Patagonian batholith: 150 my of granite magmatism on a plate margin. Lithos 97 (3-4): 373-394. https://doi.org/10.1016/j.lithos.2007.01.007

Hervé, M.; Suárez, M.; Puig, A. 1984. The Patagonian Batholith S of Tierra del Fuego, Chile: timing and tectonic implications. Journal of the Geological Society 141 (5): 909-917. https://doi.org/10.1144/gsjgs.141.5.0909

Hickey-Vargas, R.; Holbik, S.; Tormey, D.; Frey, F.; Moreno, H. 2016. Basaltic rocks from the Andean Southern Volcanic Zone: Insights from the comparison of along-strike and small-scale geochemical variations and their sources. Lithos 258-259: 115-132. https://doi.org/10.1016/j.lithos.2016.04.014

Hole, M.J. 2021. Antarctic Peninsula: Petrology. *In* Volcanism in Antarctica: 200 Million Years of Subduction, Rifting and Continental Break-Up (Smellie, J.L.; Panter, K.S.; Geyer, A.; editors). Geological Society, London, Memoir 55: 327-343. https://doi.org/10.1144/M55-2018-40

Hole, M.; Gibson, S.; Morris, M. 2023. Slab window-related magmatism as a probe for pyroxenite heterogeneities in the upper mantle. Geology 51 (3): 268-272. https://doi.org/10.1130/G50687.1

Irvine, T.N.; Baragar, W.R.A. 1971. A Guide to the Chemical Classification of the Common Volcanic Rocks. Canadian Journal of Earth Sciences 8 (5): 523-548. https://doi.org/10.1139/e71-055

Kay, S.; Ramos, V.; Márquez, M.J. 1993. Evidence in Cerro Pampa Volcanic Rocks for Slab-Melting Prior to Ridge-Trench Collision in Southern South America. The Journal of Geology 101 (6): 703-714. https://doi.org/10.1086/648269

Kilian, R.; Behrmann, J.H. 2003. Geochemical constraints on the sources of southern Chile Trench sediments and their recycling in arc magmas of the southern Andes. Journal of the Geological Society 160 (1): 57-70. https://doi.org/10.1144/0016-764901-143

Ludwig, K.R. 2000. SQUID 1.00, a user's manual. Berkeley Geochronology Center, Special Publication. Berkeley.

Moyen, J.-F. 2009. High Sr/Y and La/Yb ratios: The meaning of the "adakitic signature". Lithos 112 (3-4): 556-574. https://doi.org/10.1016/j.lithos.2009.04.001

Muller, V.A.P.; Sue, C.; Valla, P.G.; Sternai, P.; Simon-Labric, T.; Gautheron, C.; Cuffey, K.M.; Grujic, D.; Bernet, M.; Martinod, J.; Ghiglione, M.C.; Reiners, P.; Willett, C.; Shuster, D.; Herman, F.; Baumgartner, L.; Braun, J. 2024. Geodynamic and Climatic Forcing on Late-Cenozoic Exhumation of the Southern Patagonian Andes (Fitz Roy and Torres del Paine massifs). Tectonics 43 (7). https://doi.org/10.1029/2023tc007914

Müntener, O.; Kelemen, P.B.; Grove, T.L. 2001. The role of H_2O during crystallization of primitive arc magmas under uppermost mantle conditions and genesis of igneous pyroxenites: an experimental study. Contributions to Mineralogy and Petrology 141: 643-658.

Nandedkar, R.H.; Ulmer, P.; Müntener, O. 2014. Fractional crystallization of primitive hydrous arc magmas: an experimental study at 07 GPa. Contributions to Mineralogy and Petrology 167: 1015. https://doi.org/10.1007/s00410-014-1015-5

Nandedkar, R.H.; Hürlimann, N.; Ulmer, P.; Müntener, O. 2016. Amphibole-melt trace element partitioning of fractionating calc-alkaline magmas in the lower crust: an experimental study. Contributions to Mineralogy and Petrology 171 (8-9): 71. https://doi.org/10.1007/s00410-016-1278-0

Nullo, F.; Proserpio, C.; Ramos, V.; Rabassa, J. 1978. Estratigrafía y tectónica de la vertiente este del hielo continental patagónico, Argentina-Chile. *In* Congreso Geológico Argentino, No. 7 (1): 455-470.

Orihashi, Y.; Anma, R.; Motoki, A.; Haller, M.; Hirata, D.; Iwnao, H.; Sumino, H.; Ramos, V. 2013. Evolution history of the crust underlying Cerro Pampa, Argentine Patagonia: Constraint from LA-ICPMS U-Pb ages for exotic zircons in the Mid-Miocene adakite. The 120th Annual Meeting of the Geological Society of Japan, Session T3-0-09: 37 p. https://doi.org/10.14863/geosocabst.2013.0_037

Palme, H.; O'Neill, H.St.C. 2014. Cosmochemical Estimates of Mantle Composition. Treatise on Geochemistry (Second Edition) 3: 1-39. https://doi.org/10.1016/b978-0-08-095975-7.00201-1

Pardo-Casas, F.; Molnar, P. 1987. Relative motion of the Nazca (Farallon) and South American Plates since Late Cretaceous time. Tectonics 6 (3): 233-248. https://doi.org/10.1029/tc006i003p00233

Puig, A.; Hervé, M.; Suárez, M.; Saunders, A.D. 1984. Calc-alkaline and alkaline miocene and calc-alkaline recent volcanism in the Southernmost Patagonian Cordillera, Chile. Journal of Volcanology and Geothermal Research 21 (1-2): 149-163. https://doi.org/10.1016/0377-0273(84)90020-9

Ramírez de Arellano, C.; Putlitz, B.; Müntener, O.; Ovtcharova, M. 2012. High precision U/Pb zircon dating of the Chaltén Plutonic Complex (Cerro Fitz Roy, Patagonia) and its relationship to arc migration in the southernmost Andes. Tectonics 31 (4). https://doi.org/10.1029/2011tc003048

Ramírez de Arellano, C.; Calderón, M.; Rivera, H.; Valenzuela, M.; Fanning, C.M.; Paredes, E. 2021. Neogene Patagonian magmatism between the rupture of the Farallon plate and the Chile Ridge subduction. Journal of South American Earth Sciences 110: 103238. https://doi.org/10.1016/j.jsames.2021.103238

Ramos, V.A. 2005. Seismic ridge subduction and topography: Foreland deformation in the Patagonian Andes. Tectonophysics 399 (1-4): 73-86. https://doi.org/10.1016/j.tecto.2004.12.016

Ramos, V.A.; Kay, S.M. 1992. Southern Patagonian plateau basalts and deformation: Backarc testimony of ridge collisions. Tectonophysics 205 (1-3): 261-282. https://doi.org/10.1016/0040-1951(92)90430-e

Ramos, V.; Kay, S.; Singer, B. 2004. The adakites of the Patagonian Cordillera: New geochemical and geochronological evidences. Revista de la Asociación Geológica Argentina 59 (4): 693-706.

Ricci, C.; Hervé, F.; Krinauw, J.; Lemasurier, W. 1993. Naming of igneous and metamorphic rock units in Antarctica: recommendation by the SCAR Working Group on Geology. Antarctic Science 5 (1): 103-104. https://doi.org/10.1017/S0954102093000124

Salters, V.J.M.; Stracke, A. 2004. Composition of the depleted mantle. Geochemistry, Geophysics, Geosystems 5 (5). https://doi.org/10.1029/2003GC000597

Sanhueza, J.; Yáñez, G.; Buck, W.R.; Vargas, J.A.; Veloso, E. 2023. Ridge Subduction: Unraveling the Consequences Linked to a Slab Window Development Beneath South America at the Chile Triple Junction. Geochemistry, Geophysics, Geosystems 24 (9). https://doi.org/10.1029/2023gc010977

Schmidt, M.W.; Jagoutz, O. 2017. The global systematics of primitive arc melts. Geochemistry, Geophysics, Geosystems 18 (8): 2817-2854. https://doi.org/10.1002/2016gc006699

Skora, S.; Blundy, J. 2010. High-pressure Hydrous Phase Relations of Radiolarian Clay and Implications for the Involvement of Subducted Sediment in Arc Magmatism. Journal of Petrology 51 (11): 2211-2243. https://doi.org/10.1093/petrology/egq054

Stern, C.; Wit, M.J. 2003. Rocas Verdes ophiolites, southernmost South America: Remnants of progressive stages of development of oceanic-type crust in a continental margin back-arc basin. Geological Society, London, Special Publications 218: 665-683. https://doi.org/10.1144/gsl.sp.2003.218.01.32

Stevens-Goddard, A.L.; Fosdick, J.C. 2019. Multichronometer thermochronologic modeling of migrating spreading ridge subduction in southern Patagonia. Geology 47 (6): 555-558. https://doi.org/10.1130/g46091.1

Suárez, M.; Hervé, M.; Puig, Á. 1985. Hoja Isla Hoste e Islas Adyacentes, XII región. Servicio Nacional de Geología y Minería, Carta Geológica de Chile 65: 113 p., 1 mapa escala 1:250.000. Santiago.

Syracuse, E.M.; Keken, P.E. van; Abers, G.A. 2010. The global range of subduction zone thermal models. Physics of the Earth and Planetary Interiors 183 (1-2): 73-90. https://doi.org/10.1016/j.pepi.2010.02.004

Tera, F.; Wasserburg, G.J. 1972. U-Th-Pb systematics in three Apollo 14 basalts and the problem of initial Pb in lunar rocks. Earth and Planetary Science Letters 14 (3): 281-304. https://doi.org/10.1016/0012-821x(72)90128-8

Wang, X.; Sun, M.; Weinberg, R.F.; Cai, K.; Zhao, G.; Xia, X.; Li, P.; Liu, X. 2022. Adakite generation as a result of fluid-fluxed melting at normal lower crustal pressures. Earth and Planetary Science Letters 594: 117744. https://doi.org/10.1016/j.epsl.2022.117744

Williams, I. 1998. U-Th-Pb geochronology by ion microprobe. Reviews in Economic Geology 7. https://doi.org/10.5382/Rev.07.01

Wilson, M. 1989. Igneous petrogenesis a global tectonic approach. Springer Dordrecht. https://doi.org/10.1007/978-1-4020-6788-4

Xiong, X.L.; Adam, J.; Green, T.H. 2005. Rutile stability and rutile/melt HFSE partitioning during partial melting of hydrous basalt: Implications for TTG genesis. Chemical Geology 218 (3-4): 339-359. https://doi.org/10.1016/j.chemgeo.2005.01.014

Xu, J.-F.; Chen, S.-S. 2023. Petrogenesis of adakitic rocks unrelated to slab melting and adakitic porphyries associated with Cu mineralization. Lithos 458-459: 107351. https://doi.org/10.1016/j.lithos.2023.107351

Yang, S.; Su, L.; Song, S.; Allen, M.B.; Feng, D.; Wang, M.; Wang, C.; Zhang, H. 2020. Melting of subducted continental crust during collision and exhumation: Insights from granitic rocks from the North Qaidam UHP metamorphic belt, NW China. Lithos 378-379: 105794. https://doi.org/10.1016/j.lithos.2020.105794

Yogodzinski, G.M.; Lees, J.M.; Churikova, T.G.; Dorendorf, F.; Wöerner, G.; Volynets, O.N. 2001. Geochemical evidence for the melting of subducting oceanic lithosphere at plate edges. Nature 409 (6819): 500-504. https://doi.org/10.1038/35054039

Zhang, L.; Li, S.; Zhao, Q. 2021. A review of research on adakites. International Geology Review 63 (1): 47-64. https://doi.org/10.1080/00206814.2019.1702592

Zheng, Y.-F. 2019. Subduction zone geochemistry. Geoscience Frontiers 10 (4): 1223-1254. https://doi.org/10.1016/j.gsf.2019.02.003

Zhen, Z.; dong, X.; Lintao, Z. 2025. A slab window in the south rim of the Parece-Vela Basin. Scientific Reports 15 (1): 2387. https://doi.org/10.1038/s41598-025-86913-z

Manuscript received: December 02, 2025; revised/accepted: May 12, 2026; available online: May 12, 2026.